Inorganic Chemistry

pubs.acs.org/IC

Communication

Active Site Characterization of a *Campylobacter jejuni* Nitrate Reductase Variant Provides Insight into the Enzyme Mechanism

Jing Yang, Breeanna Mintmier, Khadanand KC, Mikayla C. Metzger, Manohar Radhakrishnan, Jennifer McGarry, Jarett Wilcoxen,* Partha Basu,* and Martin L. Kirk*

Cite This: *Inorg. Chem.* 2024, 63, 13191−13196

Read Online

ACCESS | Metrics & More | Article Recommendations | Supporting Information

ABSTRACT: Mo K-edge X-ray absorption spectroscopy (XAS) is used to probe the structure of wild-type *Campylobacter jejuni* nitrate reductase NapA and the C176A variant. The results of extended X-ray absorption fine structure (EXAFS) experiments on *wt* NapA support an oxidized Mo(VI) hexacoordinate active site coordinated by a single terminal oxo donor, four sulfur atoms from two separate pyranopterin dithiolene ligands, and an additional S atom from a conserved cysteine amino acid residue. We found no evidence of a terminal sulfido ligand in *wt* NapA. EXAFS analysis shows the C176A active site to be a 6-coordinate structure, and this is supported by EPR studies on C176A and small molecule analogs of Mo(V) enzyme forms. The S_{Cys} is replaced by a hydroxide or water ligand in C176A, and we find no evidence of a coordinated sulfhydryl (SH) ligand. Kinetic studies show that this variant has completely lost its catalytic activity toward nitrate. Taken together, the results support a critical role for the conserved C176 in catalysis and an oxygen atom transfer mechanism for the catalytic reduction of nitrate to nitrite that does not employ a terminal sulfido ligand in the catalytic cycle.

The periplasmic nitrate reductases (Nap)[1−3] are members of the dimethyl sulfoxide reductase (DMSOR) family of pyranopterin molybdenum enzymes and they function to convert nitrate to nitrite (Figure 1).[4−10] The DMSOR family enzymes represent the largest family of pyranopterin Mo enzymes and perform a myriad of catalytic substrate transformations[11] that include hydration,[12] oxygen atom transfer,[13,14] and formal hydride transfer reactivity.[9,15−17] The DMSOR enzyme family differs from other molybdoenzyme families in that they possess two chelating PDT (PDT = pyranopterin dithiolene) ligands[18,19] bound to the Mo ion (Figure 1, bottom) instead of the single PDT found in other pyranopterin containing molybdoenzymes. For DMSOR family enzymes, critical electronic structure and reactivity differences derive from the nature of the amino acid ligand that is coordinated to the Mo ion (e.g., Asp, Ser, Cys, or Sec) or the lack of a coordinated amino acid. Additional reactivity differences relate to whether a terminal oxo or terminal sulfido ligand is present in oxidized enzyme forms.[3,20,21] Regarding the periplasmic nitrate reductases, there is continued debate regarding the presence or absence of a sulfido or sulfido-based ligand bound the metal ion. Of these nitrate reductases, the Nap enzyme from *Campylobacter jejuni*[22−24] is of particular interest since it is an emerging antibiotic-resistant foodborne pathogen that typically colonizes the chicken gastrointestinal tract, and it can be directly transmitted to humans through food, milk, and fecal water contamination.[22] These bacterial infections can lead to severe diarrhea and, in extreme cases, death. Additionally, implications regarding human health are further impacted by documented evidence of *C. jejuni's* resistance to antibiotics.[25]

Periplasmic nitrate reductase is the only nitrate reductase found in *C. jejuni*. Coupled with the importance of *C. jejuni* in human health, this defines a critical need to understand how the geometric and electron structure of this enzyme active site contributes to nitrate reduction. Here, we employ a combination of X-ray absorption spectroscopy (XAS), extended X-ray absorption fine structure (EXAFS) data, and electron paramagnetic resonance (EPR) spectroscopy to probe the electronic and geometric structures of the *wt* NapA enzyme, the C176A variant, and relevant Mo(V) small molecule analogs. These studies address key outstanding issues regarding the nature of the terminal donor ligand to the Mo ion, the importance of the coordinated S_{Cys} in catalysis, the plasticity of the Mo-ligand coordination environment in the active site of the enzyme, and the enzyme mechanism.

The Mo K-edge XANES data (Figure 2) for both nitrate-treated *wt* NapA and as isolated C176A variant clearly indicate significant geometric and electronic structural differences between these enzyme forms. The observed differences in the near-edge spectra of *wt* NapA and the C176A variant show a shift to lower energy for the variant, and this is consistent with the C176A variant being in a more reduced state. The nature and number of the coordinating donor ligands in *wt* and C176A NapA have been determined by analyzing the Mo K-edge EXAFS data (Figure 3). The Fourier transform of the EXAFS oscillations for oxidized *wt* NapA (Figure 3A) clearly shows two peaks that are typical of terminal oxo and thiolate

Received: May 14, 2024
Revised: June 7, 2024
Accepted: June 19, 2024
Published: July 10, 2024

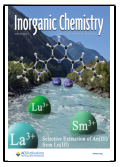

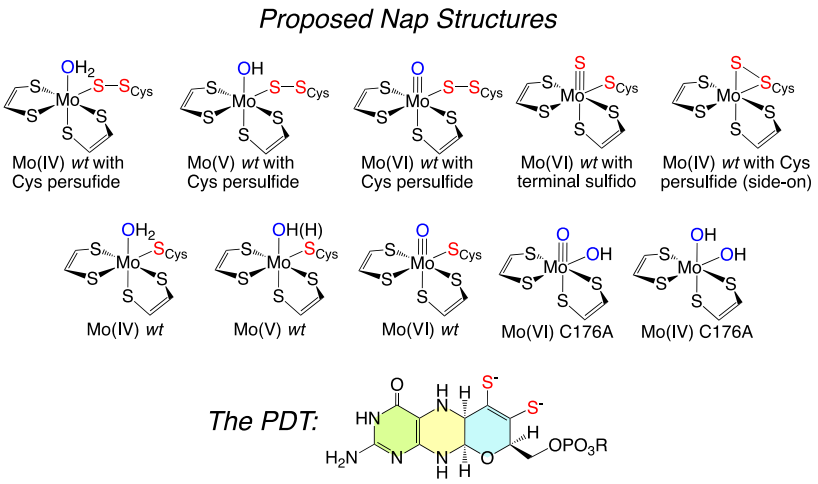

Figure 1. Top: Selected structures that have been previously proposed for sulfido-based nitrate reductase enzyme forms. Middle: Selected structures proposed for nonsulfido-based NapA enzyme forms. Bottom: Generalized structure of the reduced PDT ligand.

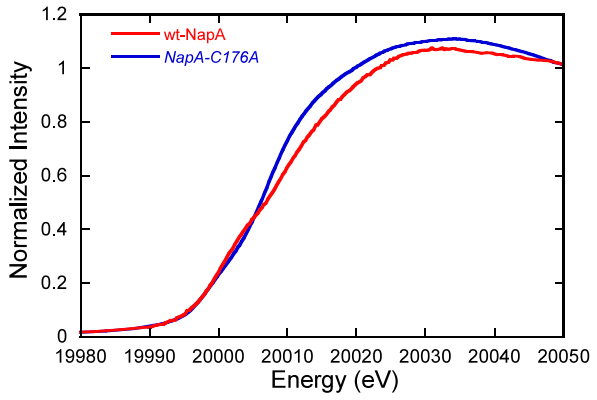

Figure 2. Mo K-edge XANES spectra for nitrate-treated *wt* NapA and its as isolated NapA-C176A variant. The rising edge energies, defined as the inflection point of the first derivative, are observed at 20014.0 eV for oxidized *wt* NapA and 20011.4 eV for NapA-C176A variant.

sulfur scatterers in molybdoenzymes and models.[26−31] The best fit to the EXAFS data gives a Mo ≡ O bond length of 1.73 Å, an average dithiolene Mo−S bond lengths of 2.44 Å, and four second coordination sphere dithiolene C scatterers at 3.34 Å (Figure 3A,B). The computational model used for the EXAFS fit is shown in Figure 3C. As anticipated from the differences in the XANES data, the Fourier transform of the EXAFS oscillations for the NapA-C176A variant is quite different from that of the *wt* enzyme. Namely, the EXAFS intensity in the region of the terminal oxo scatterer is markedly reduced compared to that observed in the *wt* data. The best fit to the EXAFS data for the C176A variant (Figure 3D,E) yields a single oxo scatterer with a Mo ≡ O bond length of 1.71 Å, a single Mo−OH(H) bond at 2.05 Å, and four Mo−S bonds from the two PDT dithiolene ligands at 2.37 Å. The computational model used for the EXAFS fit is depicted in Figure 3F. Interestingly, a very similar $[(PDT)_2Mo^{4+}O(O-As)]^{-1}$ mono-oxo structure was determined by EXAFS for reduced arsenite oxidase (Alphaproteobacterium *Rhizobium* sp. str. NT-26).[32] Similar to the NapA C176A variant, arsenite oxidase does not possess an amino acid donor bound to the Mo site. Our analysis of the data for the C176A variant shows that the reduction in the terminal oxo scattering peak height relative to *wt* enzyme results from a larger Debye−Waller factor (σ^2 = 0.010 Å^2), indicating some static disorder involving the terminal oxo ligand.[33] We hypothesize that this larger Debye−Waller factor derives from the lack of a coordinating amino acid residue in the C176A variant leading to a markedly more conformationally flexible active site than is present in the *wt* enzyme.

Our NapA XAS results indicate both *wt* enzyme and the C176A variant possess a terminal oxo ligand. This is important since a terminal sulfido ligand (Figure 1) has been suggested to play a critical mechanistic role in both nitrate reductases and formate dehydrogenases[3,34] via the formation of a cysteine persulfide ligand. This has been referred to as the sulfur-shift mechanism[1,34] and leads to the two-electron reduction of Mo and an open coordination site to bind H_2O/OH^- or the nitrate substrate in the reduced Mo(IV) state (Figure 1). Although our work clearly shows that oxidized *wt* Nap lacks a terminal sulfido ligand, the EXAFS data are consistent with either a $[(PDT)_2MoO(S\text{-}R_{Cys})]^{1-}$ structure, with a coordinated cysteine thiolate, or a $[(PDT)_2MoO(S{-}S\text{-}R_{Cys})]^{1-}$ active site structure with a terminal persulfide ligand.[35] In marked contrast to *wt* NapA, the C176A NapA variant (Figure 1) is incapable of forming a cysteine persulfide since it lacks a cysteine thiolate ligand. If a sulfur-shift mechanism were to be operative in NapA, the C176A variant would be expected to possess a terminal sulfido ligand in the oxidized state. Similarly, the reduced Mo(IV) form would be expected to possess a sulfhydryl ligand. Neither of these structures are supported by our analysis of the C176A NapA EXAFS data. Thus, the lack of a terminal sulfido derived ligand in the C176A variant strongly suggests an alternative mechanism for nitrate reduction in *C. jejuni* NapA.

EPR spectroscopic studies on the oxidized C176A variant show that these samples contain some one-electron reduced Mo(V) species (Figure 4, top). The C176A EPR spectra are very similar to EPR data obtained for the C148A variant of *Synechococcus sp.* PCC 7942 cytoplasmic nitrate reductase (NarB; $g_{1,2,3}$ = 2.025, 1.990, 1.970), which has been suggested to possess an active site structure very similar to *C. jejuni* NapA.[36] EPR spectra of DMSOR family molybdoenzymes reveal important information regarding the electronic and geometric structure of the Mo center, and the ligands bound to the Mo ion.[14,30,37−40] To gain additional insight into the structure of the C176A Mo(V) species, we compare the

https://doi.org/10.1021/acs.inorgchem.4c01991
Inorg. Chem. 2024, 63, 13191−13196

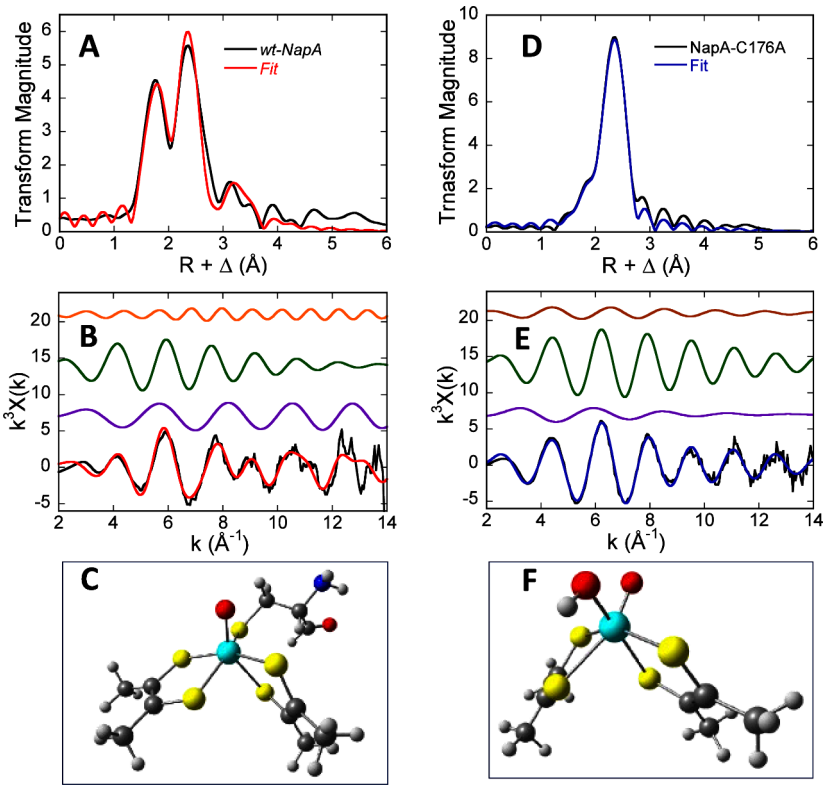

Figure 3. Mo K-edge EXAFS data for oxidized *wt* NapA (A and B) and the NapA-C176A variant (D and E). The experimental data are shown in black, and the best fits to the data are in red for *wt* NapA and blue for NapA-C176A. Four Mo−C scatters from the dithiolene C═C carbon atoms of the two PDT ligands have been included in the fit for *wt* NapA, yielding Mo−C vectors at an average distance of 3.34 Å. The observed oscillations arise from terminal oxo, S, C (second coordination sphere), and OH scatterers and are colored in purple, green, orange, and brown, respectively. Fits to the EXAFS data for *wt* NapA and the C176A variant used the computational models shown in C and F, respectively. The XAS data for the *wt* protein was obtained by incubating the enzyme with nitrate.

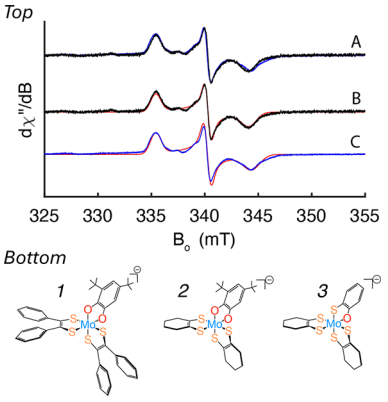

Figure 4. Top: X-band EPR spectra of the as-isolated NapA C176A variant in H_2O (black) and D_2O (blue) (50 mM HEPES pH 7.4) with simulations of the spectra in red. Enzyme concentrations are approximately 200 μM. The spectra in H_2O and D_2O buffer are virtually identical (A) and show no evidence for strongly coupled protons. EPR spin quantitation yields ∼10−20% of the variant being in the Mo(V) oxidation state (see SI). The g-values determined from spectral simulations are $g_{1,2,3}$ = 2.0170, 1.9876, 1.9644 in H_2O sample (B) and $g_{1,2,3}$ = 2.0178, 1.9888, 1.9645 in D_2O (C). Bottom: Bond line drawings for small molecule analogs of the Mo(V) forms of C176A NapA (**1**−**2**) and *wt* NapA (**3**).

C176A EPR spin-Hamiltonian parameters ($g_{1,2,3}$ = 2.0172, 1.9879, 1.9647), derived from spectral simulations of the data in Figure 4, with three small molecule analogs (**1**-**3**; Figure 4, bottom) of the Mo(V) NapA site (Table S1). The EPR g-values for C176A NapA are remarkably similar to the Mo(V) coordination environments previously determined for the model compounds **1** ($g_{1,2,3}$ = 2.0066, 1.9881, 1.9655) and **2** ($g_{1,2,3}$ = 2.0110, 1.9856, 1.9636) that lack a terminal oxo ligand.[29] The presence of two hydroxide ligands in the putative $[(PDT)_2Mo^{V}(OH)_2]^{1-}$ structure for C176A NapA have been modeled in **1** and **2** using a catecholate ligand.[29] The EPR g-values for C176A NapA are also similar to those determined for *lpH* Nar,[41,42] *Rs* DorA,[14] and MtsZ form 1,[37] all of which possess $[(PDT)_2Mo^{V}(OH)(OR)]^{1-}$ first coordination sphere geometries (OR = serinate or aspartate). Compound **3** is a model for a $[(PDT)_2Mo^{V}(SH)(OH)]^{1-}$ structure that contains a protonated terminal sulfido (i.e., sulfhydryl) ligand (see SI). Here, the presence of an additional sulfur donor leads to a larger value for g_3 ($g_{1,2,3}$ = 2.0110, 1.9908, 1.9836) and a markedly more axial spectrum (Figure S1) when compared to compounds **1** and **2**, and the Mo(V) form of C176A NapA (Figure S1). The different EPR g-values for **3** and C176A NapA are consistent with the fact that the C176A variant does not possess a coordinated cysteine thiolate, and these data argue strongly against a protonated terminal sulfido (sulfhydryl) ligand in the paramagnetic Mo(V) forms of the enzyme.

Taken together, the results of this study demonstrate the presence of a terminal oxo ligand in oxidized *wt C. jejuni* NapA, as opposed to a terminal sulfido ligand coordinated to the Mo ion. Additionally, the EXAFS and EPR data on the C176A variant indicate that neither a sulfido nor a sulfhydryl ligand is present in this enzyme form. Our results point to a

https://doi.org/10.1021/acs.inorgchem.4c01991
Inorg. Chem. 2024, 63, 13191−13196

$[(PDT)_2Mo^{VI}O(S_{Cys})]^{1-}$ active site structure for oxidized *C. jejuni* NapA, and inorganic sulfur is not present as a component of sulfido, persulfido, or sulfhydryl ligation. The presence of a terminal oxo ligand in the *wt* enzyme, coupled with the lack of a terminal sulfido donor, points to an oxygen atom transfer mechanism for NapA as suggested by Dias et al.[43] Our data allow us to propose a mechanism (Figure 5) that

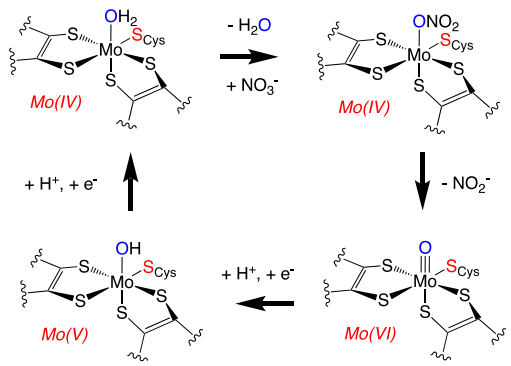

Figure 5. Proposed NapA oxygen atom transfer mechanism based on the results of this study.

starts from a $[(PDT)_2Mo^{4+}(OH_2)(S_{Cys})]^{1-}$ resting state, which can subsequently lose a labile aqua ligand prior to binding substrate to form $[(PDT)_2Mo^{4+}(NO_3)(S_{Cys})]^{2-}$. This direct oxygen atom transfer mechanism is consistent with previously determined kinetic parameters for this enzyme, where the catalytic efficiency of the *wt* enzyme is 1.64×10^6 M^{-1} s^{-1}.[24] The catalytic efficiency is reduced by 4 orders of magnitude in the C176S and C176D NapA variants,[24] and the C176A NapA variant is completely inactive toward nitrate. Additionally, we have recently determined that cyanide acts as a noncompetitive inhibitor of *Cj* NapA.[44] This result indicates that cyanide does not bind at the active site and does not function as either a competitive inhibitor or as a suicide inhibitor by reacting with a terminal sulfido ligand (i.e., cyanolysis). These results underscore the importance of direct cysteine coordination to the molybdenum center,[45] the lack of a terminal sulfido ligand, and the presence of a coordinated terminal oxo ligand for oxygen atom transfer reactivity in *Cj* NapA.

■ ASSOCIATED CONTENT

Supporting Information

The Supporting Information is available free of charge at https://pubs.acs.org/doi/10.1021/acs.inorgchem.4c01991.

NapA protein production and preparation, model compound synthesis and characterization data, EPR spectra, EXAFS details and data, and computational coordinates (PDF)

■ AUTHOR INFORMATION

Corresponding Authors

Jarett Wilcoxen − *Department of Chemistry and Biochemistry, University of Wisconsin, Milwaukee, Wisconsin 53211, United States;* orcid.org/0000-0003-2220-0815; Email: jarettw@uwm.edu

Partha Basu − *Department of Chemistry and Chemical Biology, Indiana University, Indianapolis, Indiana 46202, United States;* orcid.org/0000-0002-1232-418X; Email: basup@iu.edu

Martin L. Kirk − *Department of Chemistry and Chemical Biology, The University of New Mexico, Albuquerque, New Mexico 87131-0001, United States;* orcid.org/0000-0002-1479-3318; Email: mkirk@unm.edu

Authors

Jing Yang − *Department of Chemistry and Chemical Biology, The University of New Mexico, Albuquerque, New Mexico 87131-0001, United States;* orcid.org/0000-0001-8241-9160

Breeanna Mintmier − *Department of Chemistry and Chemical Biology, Indiana University, Indianapolis, Indiana 46202, United States*

Khadanand KC − *Department of Chemistry and Chemical Biology, The University of New Mexico, Albuquerque, New Mexico 87131-0001, United States;* orcid.org/0000-0002-1258-8636

Mikayla C. Metzger − *Department of Chemistry and Chemical Biology, Indiana University, Indianapolis, Indiana 46202, United States*

Manohar Radhakrishnan − *Department of Chemistry and Chemical Biology, Indiana University, Indianapolis, Indiana 46202, United States*

Jennifer McGarry − *Department of Chemistry and Biochemistry, University of Wisconsin, Milwaukee, Wisconsin 53211, United States; Department of Chemistry and Chemical Biology, Indiana University, Indianapolis, Indiana 46202, United States*

Complete contact information is available at: https://pubs.acs.org/10.1021/acs.inorgchem.4c01991

Notes

The authors declare no competing financial interest.

■ ACKNOWLEDGMENTS

M.L.K. acknowledges the National Institutes of Health (GM-057378) for continued financial support of our work on molybdoenzymes and models. M.L.K. and J.Y. acknowledge SSRL staff members Erik Nelson, Matthew Latimer, and Leah Kelly for their assistance and help with the collection of the XAS data. Use of the Stanford Synchrotron Radiation Lightsource and SLAC National Accelerator Laboratory is supported by the U.S. Department of Energy, Office of Science, Office of Basic Energy Sciences under Contract No. DE-AC02-76SF00515. The authors thank the UNM Center for Advanced Research Computing, supported in part by the National Science Foundation, for providing high performance computing resources used in this work. P.B. acknowledges financial support from the National Science Foundation (CHE 2003752) and the National Institutes of Health (GM 139064) for partial financial support of this work.

■ REFERENCES

(1) Cerqueira, N.; Fernandes, P. A.; Gonzalez, P. J.; Moura, J. J. G.; Ramos, M. J. The Sulfur Shift: An Activation Mechanism for Periplasmic Nitrate Reductase and Formate Dehydrogenase. *Inorg. Chem.* **2013**, *52* (19), 10766−10772.

(2) Sparacino-Watkins, C.; Stolz, J. F.; Basu, P. Nitrate and periplasmic nitrate reductases. *Chem. Soc. Rev.* **2014**, *43* (2), 676−706.

(3) Cerqueira, N.; Gonzalez, P. J.; Fernandes, P. A.; Moura, J. J. G.; Ramos, M. J. Periplasmic Nitrate Reductase and Formate Dehydrogenase: Similar Molecular Architectures with Very Different Enzymatic Activities. *Acc. Chem. Res.* **2015**, *48* (11), 2875−2884.

(4) Hille, R.; Hall, J.; Basu, P. The Mononuclear Molybdenum Enzymes. *Chem. Rev.* **2014**, *114* (7), 3963−4038.
(5) Hille, R.; Schulzke, C.; Kirk, M. L. *Molybdenum and Tungsten Enzymes*; RSC Metallobiology Series; Garner, C. D., Sun, H., Wedd, A., Ciurli, S. L., Eds.; The Royal Society of Chemistry: Cambridge, UK, 2017.
(6) Kirk, M. L.; Hille, R. Spectroscopic Studies of Mononuclear Molybdenum Enzyme Centers. *MOLECULES* **2022**, *27* (15), 4802.
(7) Ingersol, L. J.; Kirk, M. L. Structure, Function, and Mechanism of Pyranopterin Molybdenum and Tungsten Enzymes. In *Comprehensive Coordination Chemistry III*; Constable, E. C., Parkin, G., Que, L., Jr., Eds.; Elsevier, 2021; pp 790−811.
(8) Kirk, M. L.; Kc, K. Molybdenum and Tungsten Cofactors and the Reactions They Catalyze. In *Metal Ions in Life Sciences*; Sosa Torres, M., Kroneck, P., Eds.; Vol. 20; De Gruyter, 2020; pp 313−342.
(9) Kirk, M. L. Spectroscopic and Electronic Structure Studies Probing Mechanism: Introduction and Overview. In *Molybdenum and Tungsten Enzymes: Spectroscopic and Theoretical Investigations*; The Royal Society of Chemistry, 2017; pp 1−12.
(10) Kirk, M. L.; Stein, B. The Molybdenum Enzymes. In *Comprehensive Inorganic Chemistry II*, second ed.; Jan, R., Kenneth, P., Eds.; Elsevier, 2013; pp 263−293.
(11) Le, C.; Bae, M.; Kiamehr, S.; Balskus, E. P. Emerging Chemical Diversity and Potential Applications of Enzymes in the DMSO Reductase Superfamily. *Annu. Rev. Biochem.* **2022**, *91*, 475−504.
(12) Kroneck, P. M. H. Acetylene hydratase: a non-redox enzyme with tungsten and iron-sulfur centers at the active site. *Journal of Biological Inorganic Chemistry* **2016**, *21* (1), 29−38.
(13) Holm, R. H.; Solomon, E. I.; Majumdar, A.; Tenderholt, A. Comparative molecular chemistry of molybdenum and tungsten and its relation to hydroxylase and oxotransferase enzymes. *Coord. Chem. Rev.* **2011**, *255* (9), 993−1015.
(14) Mtei, R. P.; Lyashenko, G.; Stein, B.; Rubie, N.; Hille, R.; Kirk, M. L. Spectroscopic and Electronic Structure Studies of a Dimethyl Sulfoxide Reductase Catalytic Intermediate: Implications for Electron- and Atom-Transfer Reactivity. *J. Am. Chem. Soc.* **2011**, *133* (25), 9762−9774.
(15) Graham, J. E.; Niks, D.; Zane, G. M.; Gui, Q.; Hom, K.; Hille, R.; Wall, J. D.; Raman, C. S. How a Formate Dehydrogenase Responds to Oxygen: Unexpected O2 Insensitivity of an Enzyme Harboring Tungstopterin, Selenocysteine, and [4Fe−4S] Clusters. *ACS Catal.* **2022**, *12* (16), 10449−10471.
(16) Niks, D.; Duvvuru, J.; Escalona, M.; Hille, R. Spectroscopic and Kinetic Properties of the Molybdenum-containing, NAD+-dependent Formate Dehydrogenase from Ralstonia eutropha. *J. Biol. Chem.* **2016**, *291*, 1162.
(17) Niks, D.; Hille, R. Molybdenum- and tungsten-containing formate dehydrogenases and formylmethanofuran dehydrogenases: Structure, mechanism, and cofactor insertion. *Protein Sci.* **2019**, *28* (1), 111−122.
(18) Burgmayer, S. J. N.; Kirk, M. L. Advancing Our Understanding of Pyranopterin-Dithiolene Contributions to Moco Enzyme Catalysis. *Molecules* **2023**, *28*, 7456.
(19) Rothery, R. A.; Stein, B.; Solomonson, M.; Kirk, M. L.; Weiner, J. H. Pyranopterin conformation defines the function of molybdenum and tungsten enzymes. *Proc. Natl. Acad. Sci. U. S. A.* **2012**, *109* (37), 14773−14778.
(20) Coelho, C.; Gonzalez, P. J.; Moura, J. J. G.; Moura, I.; Trincao, J.; Romao, M. J. The Crystal Structure of Cupriavidus necator Nitrate Reductase in Oxidized and Partially Reduced States. *J. Mol. Biol.* **2011**, *408* (5), 932−948.
(21) Cerqueira, N.; Gonzalez, P. J.; Brondino, C. D.; Romao, M. J.; Romao, C. C.; Moura, I.; Moura, J. J. G. The Effect of the Sixth Sulfur Ligand in the Catalytic Mechanism of Periplasmic Nitrate Reductase. *J. Comput. Chem.* **2009**, *30* (15), 2466−2484.
(22) Elmi, A.; Nasher, F.; Dorrell, N.; Wren, B.; Gundogdu, O. Revisiting *Campylobacter jejuni* Virulence and Fitness Factors: Role in Sensing, Adapting, and Competing. *Frontiers in Cellular and Infection Microbiology* **2021**, *10*, na DOI: 10.3389/fcimb.2020.607704.
(23) Zhong, Q.; Kobe, B.; Kappler, U. Molybdenum Enzymes and How They Support Virulence in Pathogenic Bacteria. *Frontiers in Microbiology* **2020**, *11*, Review.
(24) Mintmier, B.; McGarry, J. M.; Sparacino-Watkins, C. E.; Sallmen, J.; Fischer-Schrader, K.; Magalon, A.; McCormick, J. R.; Stolz, J. F.; Schwarz, G.; Bain, D. J.; et al. Molecular cloning, expression and biochemical characterization of periplasmic nitrate reductase from Campylobacter jejuni. *FEMS Microbiol. Lett.* **2018**, *365* (16), fny151−fny151.
(25) European Food Safety. The European Union Summary Report on Antimicrobial Resistance in zoonotic and indicator bacteria from humans, animals and food in 2019−2020. *EFSA Journal* **2022**, *20* (3), na.
(26) George, G. N. X-Ray Absorption Spectroscopy of Molybdenum and Tungsten Enzymesons. In *Molybdenum and Tungsten Enzymes: Spectroscopic and Theoretical Investigation*; Hille, R., Schulzke, C., Kirk, M. L., Eds.; The Royal Society of Chemistry, 2017; pp 121−167.
(27) Pushie, M. J.; George, G. N. Spectroscopic studies of molybdenum and tungsten enzymes. *Coord. Chem. Rev.* **2011**, *255* (9−10), 1055−1084.
(28) Harris, H. H.; George, G. N.; Rajagopalan, K. V. High-Resolution EXAFS of the Active Site of Human Sulfite Oxidase: Comparison with Density Functional Theory and X-ray Crystallographic Results. *Inorg. Chem.* **2006**, *45*, 493−495.
(29) Kc, K.; Yang, J.; Kirk, M. L. Addressing Serine Lability in a Paramagnetic Dimethyl Sulfoxide Reductase Catalytic Intermediate. *Inorg. Chem.* **2021**, *60* (13), 9233−9237.
(30) Ingersol, L. J.; Yang, J.; KC, K.; Pokhrel, A.; Astashkin, A. V.; Weiner, J. H.; Johnston, C. A.; Kirk, M. L. Addressing Ligand-Based Redox in Molybdenum-Dependent Methionine Sulfoxide Reductase. *J. Am. Chem. Soc.* **2020**, *142* (6), 2721−2725.
(31) Yang, J.; Struwe, M.; Scheidig, A.; Mengell, J.; Clement, B.; Kirk, M. L. Active Site Structures of the Escherichia coli N-Hydroxylaminopurine Resistance Molybdoenzyme YcbX. *Inorg. Chem.* **2023**, *62* (14), 5315−5319.
(32) Warelow, T. P.; Pushie, M. J.; Cotelesage, J. J. H.; Santini, J. M.; George, G. N. The active site structure and catalytic mechanism of arsenite oxidase. *Sci. Rep.* **2017**, *7* (1), 1757.
(33) Furuta, S.; Miyanaga, T.; Watanabe, I. An Abnormally Large EXAFS Debye-Waller Factor for a Mo−O Bond in Hexamolybdate. *AIP Conf. Proc.* **2007**, *882* (1), 141−143.
(34) Leimkühler, S. Metal-Containing Formate Dehydrogenases, a Personal View. *Molecules* **2023**, *28*, 5338.
(35) Giles, L. J.; Ruppelt, C.; Yang, J.; Mendel, R. R.; Bittner, F.; Kirk, M. L. Molybdenum Site Structure of MOSC Family Proteins. *Inorg. Chem.* **2014**, *53* (18), 9460−9462.
(36) Srivastava, A. P.; Allen, J. P.; Vaccaro, B. J.; Hirasawa, M.; Alkul, S.; Johnson, M. K.; Knaff, D. B. Identification of Amino Acids at the Catalytic Site of a Ferredoxin-Dependent Cyanobacterial Nitrate Reductase. *Biochemistry* **2015**, *54* (36), 5557−5568.
(37) Struwe, M. A.; Kalimuthu, P.; Luo, Z. Y.; Zhong, Q. F.; Ellis, D.; Yang, J.; Khadanand, K. C.; Harmer, J. R.; Kirk, M. L.; McEwan, A. G. Active site architecture reveals coordination sphere flexibility and specificity determinants in a group of closely related molybdoenzymes. *J. Biol. Chem.* **2021**, *296*, 100672.
(38) Grimaldi, S.; Biaso, F.; Burlat, B.; Guigliarelli, B. Electron Paramagnetic Resonance Studies of Molybdenum Enzymes. In *Molybdenum and Tungsten Enzymes: Biochemistry*; Hille, R., Schulzke, C., Kirk, M. L., Eds.; Vol. 5; The Royal Society of Chemistry, 2017.
(39) Yang, J.; Giles, L. J.; Ruppelt, C.; Mendel, R. R.; Bittner, F.; Kirk, M. L. Oxyl and Hydroxyl Radical Transfer in Mitochondrial Amidoxime Reducing Component-Catalyzed Nitrite Reduction. *J. Am. Chem. Soc.* **2015**, *137* (16), 5276−5279.
(40) Manikandan, P.; Choi, E.; Hille, R.; Hoffman, B. 35 GHz ENDOR characterization of the ″very rapid″ signal of xanthine oxidase reacted with 2-hydroxy-6-methylpurine ((13)C8): Evidence

against direct Mo-C8 interaction. *J. Am. Chem. Soc.* **2001**, *123* (11), 2658−2663.
(41) Rendon, J.; Biaso, F.; Ceccaldi, P.; Toci, R.; Seduk, F.; Magalon, A.; Guigliarelli, B.; Grimaldi, S. Elucidating the Structures of the Low- and High-pH Mo(V) Species in Respiratory Nitrate Reductase: A Combined EPR, 14,15N HYSCORE, and DFT Study. *Inorg. Chem.* **2017**, *56* (8), 4422−4434.
(42) Vincent, S. P.; Bray, R. C. Electron-Paramagnetic-Resonance Studies on Nitrate Reductase from *Escherichia coli* K12. *Biochem. J.* **1978**, *171*, 639−647.
(43) Dias, J. M.; Than, M. E.; Humm, A.; Huber, R.; Bourenkov, G. P.; Bartunik, H. D.; Bursakov, S.; Calvete, J.; Caldeira, J.; Carneiro, C.; et al. Crystal Structure of the First Dissimilatory Nitrate Reductase at 1.9 Å Solved by Multiwavelength Anomalous Diffraction Methods. *Structure* **1999**, *7*, 65−79.
(44) Giri, N. C.; Mintmier, B.; Radhakrishnan, M.; Mielke, J.; Wilcoxen, J.; Basu, P. The critical role of a conserved lysine residue in periplasmic nitrate reductase catalyzed reactions. *JBIC J. Biol. Inorg. Chem.* **2024**, *29*, 395.
(45) Mintmier, B.; McGarry, J. M.; Bain, D. J.; Basu, P. Kinetic consequences of the endogenous ligand to molybdenum in the DMSO reductase family: a case study with periplasmic nitrate reductase. *Journal of Biological Inorganic Chemistry* **2021**, *26* (1), 13−28.

https://doi.org/10.1021/acs.inorgchem.4c01991
Inorg. Chem. 2024, 63, 13191−13196